Civil 5730 Term Project

Modified Cam-Clay Model for Soil Behavior Simulation under Triaxial Condition by Explicit Integration Method

Student Name : Yu Zhijie

Student ID : 20454611

Email Address : zyuak@connect.ust.hk

Due Date : 2018/May/24

1. Abstract

The modified cam-clay model (MCC) was first introduced by Roscoe and Burland (1968), which has become one of the most widely used soil constitutive models in scientific researches and practical engineering. The MCC model has an elliptic yield surface on the *p'*-q plane, and at the same time, the associative flow rule and strain hardening law are adopted by the model.

To investigate the reliability of the MCC model, first, three undrained triaxial tests carried out numerically using the explicit stress-integration method. The soil parameters utilized in the simulation were calibrated based on the experiment data. The simulation results were then compared with the experiment result and the good agreement between simulation and experiment can be found to some extent. It can be concluded that the MCC model is accurate enough in simulating the soil behavior in this special case.

Next, the soil behavior under cyclic loading was also predicted using the MCC model. The predicted soil behavior seems different from which measured in experiments. Little hysteresis effects could be found in the simulation result. That may indicate that the MCC model is not suitable for simulating soil behavior under cyclic loading.

2. Introduction of the MCC Model

The modified cam-clay model (MCC) was proposed by Roscoe and Burlandin (1968), which is now commonly referred to as Cam-Clay model. It is an extension and modification of the Original Cam-Clay model which is introduced by Roscoe *et al.* in 1958 and 1963. In this project, the model will be described in term of the mean effective stress *p'* and deviatoric stress *q*.

2.1. Yield function

Assuming the plastic work rate (equal to the rate of dissipation energy) is

$$dW^p = p' d\varepsilon_v^p + q d\varepsilon_q^p = p' \sqrt{\left(d\varepsilon_v^p\right)^2 + \left(M d\varepsilon_q^p\right)^2} \tag{2.1}$$

Based on this assumption and using the associative flow rule, the yield function of the MCC model can be derived as the following

$$f = M^2 p'^2 - M^2 p_0' p' + q^2 = 0 \tag{2.2}$$

where

M = the stress ratio q/p' at the critical state line; and

p_0' = the pre-consolidation pressure.

The yield surface on p'-q plane is an ellipse in shape and ellipsoidal shape in the general 3D principal stress space, as shown in Fig. 1.

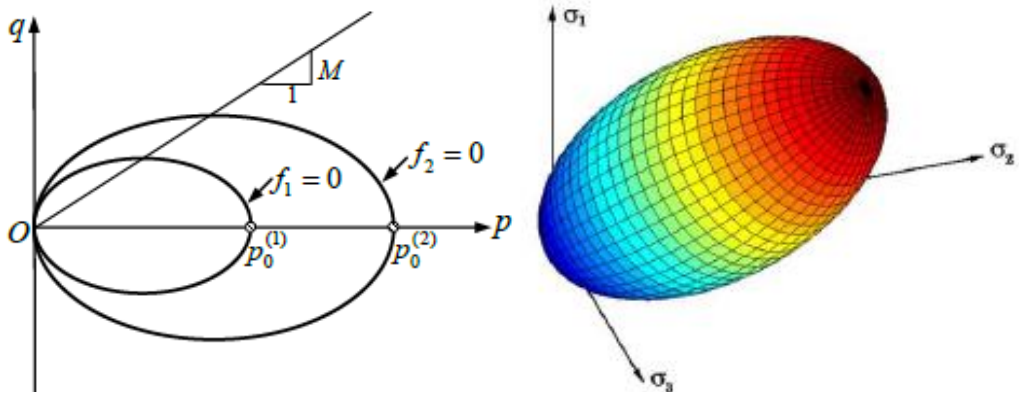

Fig. 1 Yielding surface in the p'-q space and 3D principal stress space

2.2. State Variable: Initial mean effective stress

Usually the plastic volumetric strain can be considered as a state variable.

$$d\varepsilon_v^p = \langle L \rangle \left(\frac{\partial f}{\partial p'} \frac{\partial p'}{\partial \sigma_{kk}} + \frac{\partial f}{\partial q} \frac{\partial q}{\partial \sigma_{kk}} \right) = \langle L \rangle M^2 (2p' - p_0') \tag{2.3}$$

p_0' is the initial mean effective stress of a soil sample.

But considering the yield function of MCC in (2.2), p_0' is obviously more explicit than ε_v^p, so in this report the initial mean effective stress p_0' is chosen as the state variable known as the hardening parameter

$$dp_0' = p_0' \frac{1+e_0}{\lambda - \kappa} d\varepsilon_v^p = \langle L \rangle p_0' \frac{1+e_0}{\lambda - \kappa} \left(\frac{\partial f}{\partial p'} \frac{\partial p'}{\partial \sigma_{kk}} + \frac{\partial f}{\partial q} \frac{\partial q}{\partial \sigma_{kk}} \right) \tag{2.4}$$

2.3. Plastic Modulus

The plastic modulus for the modified cam-clay model is

$$K_p = \frac{\partial f}{\partial \varepsilon_v^p} M^2 (2p' - p_0') = M^4 \frac{1+e_0}{\lambda - \kappa} p_0' (2p' - p_0') \tag{2.5}$$

2.4. Elastic stress-strain relation

The generalized Hooke's law can be utilized to describe the elastic stress-strain relation for the modified cam-clay model.

$$\begin{Bmatrix} dp' \\ dq \end{Bmatrix} = \begin{bmatrix} K & 0 \\ 0 & 3G \end{bmatrix} \begin{Bmatrix} d\varepsilon_v^e \\ d\varepsilon_q^e \end{Bmatrix} \tag{2.6}$$

where

$K = \frac{1+e_0}{\kappa} p'$, is the elastic bulk modulus; and

$G = \frac{3(1-2\nu)}{2(1+\nu)} K$, is the shear modulus.

However, experimental data show that soil's shear modulus is in general not proportional to *p'*, so the Poisson's ratio is also a function of *p'*.

2.5. Elastoplastic stiffness matrix

In order to obtain the elstoplastic stiffness matrix, $\frac{\partial f}{\partial \sigma_{ij}}$ have to be evaluated.

$$\frac{\partial f}{\partial \sigma_{ij}} = \frac{\partial f}{\partial p'} \frac{\partial p'}{\partial \sigma_{ij}} + \frac{\partial f}{\partial q} \frac{\partial q}{\partial \sigma_{ij}} = M^2 (2p' - p_0') \frac{\partial p'}{\partial \sigma_{ij}} + 2q \frac{\partial q}{\partial \sigma_{ij}} \tag{2.7}$$

Then, the elastoplastic stiffness matrix can be evaluated using Equation (2.8).

$$D_{ijkl} = C_{ijkl} - h(L) \frac{\left(C_{ijmn} \frac{\partial f}{\partial \sigma_{mn}} \right) \left(\frac{\partial f}{\partial \sigma_{pq}} C_{ipqkl} \right)}{\frac{\partial f}{\partial \sigma_{ab}} C_{iabcd} \frac{\partial f}{\partial \sigma_{cd}} + K_p} \tag{2.8}$$

Where,

K_p = the plastic bulk modulus which can be calculated using Equation (2.5);

C_{ijkl} = the elastic stiffness matrix;

$L = \frac{a^T D_e d\varepsilon}{a^T D_e a + K_p}$, is the loading index; and

$$h(L)=\begin{cases}1 & if\ L>0\\ 0 & otherwise\end{cases}$$

3. Description of the Explicit Method in the self-written code

To realize the explicit stress-integration method of the MCC model, a self-written code is finished using Python edited by Jupyter Notebook. The flow chart of the modified Regula-Falsi intersection scheme is illustrated as Fig. 2.

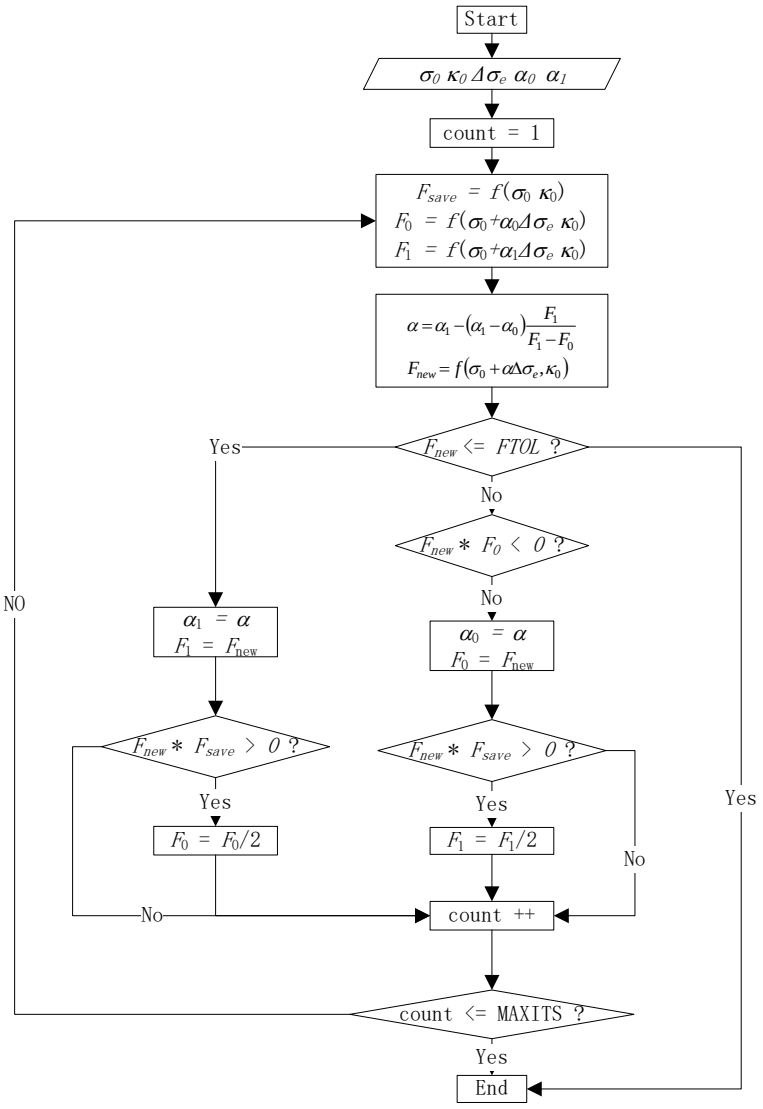

Fig. 2 Flow chart of the modified Regula-Falsi intersection scheme

The flow chart of the modified Regula-Falsi intersection scheme for negative plastic multiplier is presented in Fig. 3.

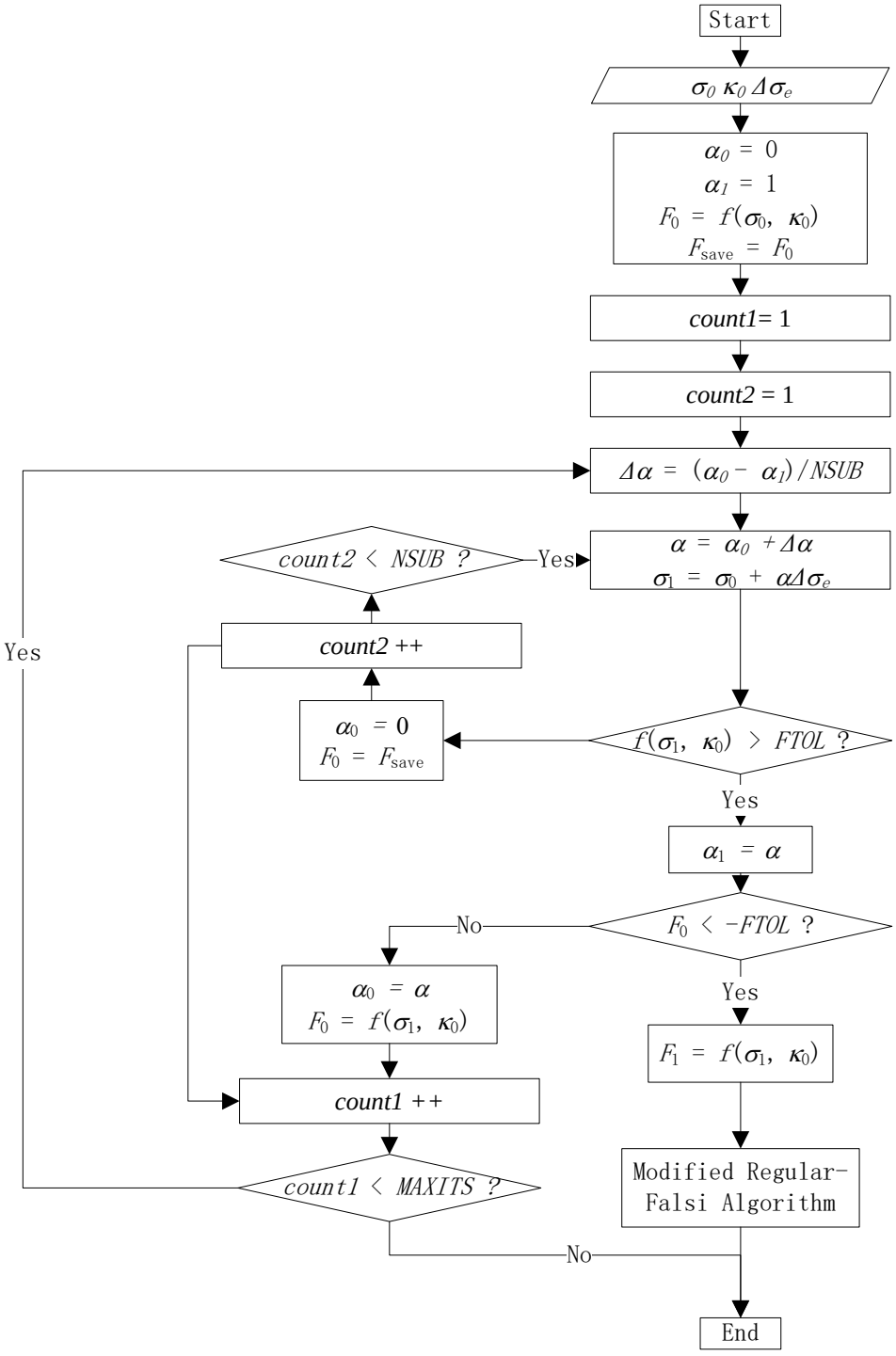

Fig. 3 Flow chart of the modified Regula-Falsi intersection scheme for negative multiplier

The flow chart of the yield surface drift correction scheme is illustrated as Fig. 4.

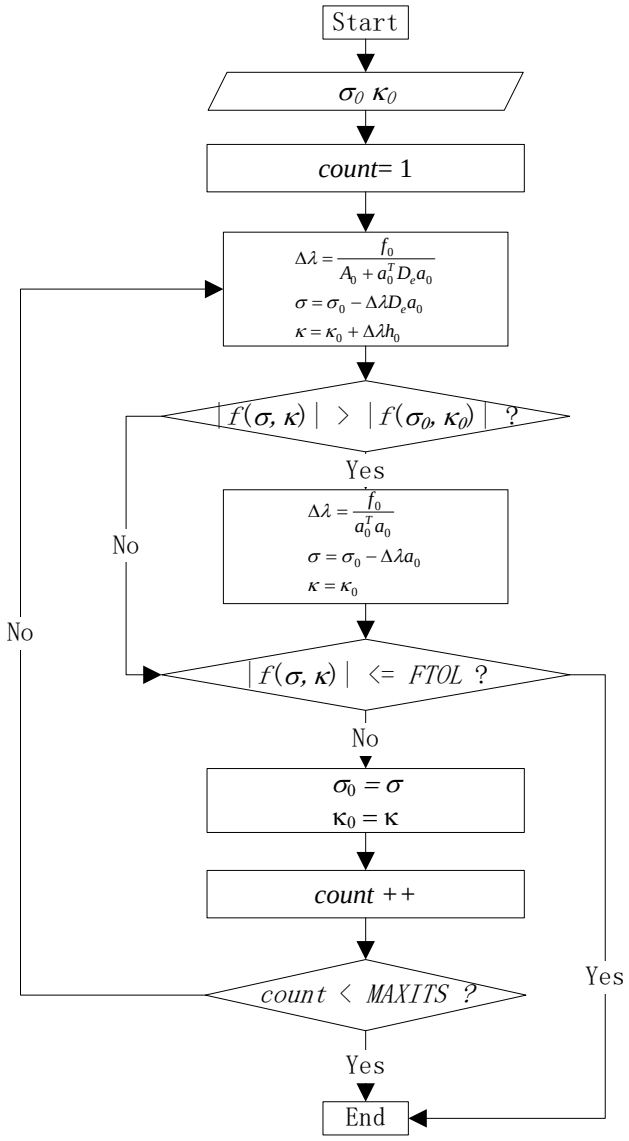

Fig. 4 Flow chart of the the yield surface drift correction scheme

The flow chart of the whole explicit method is described as Fig. 5. The sub-algorithm can be referred to Fig. 2 to 4.

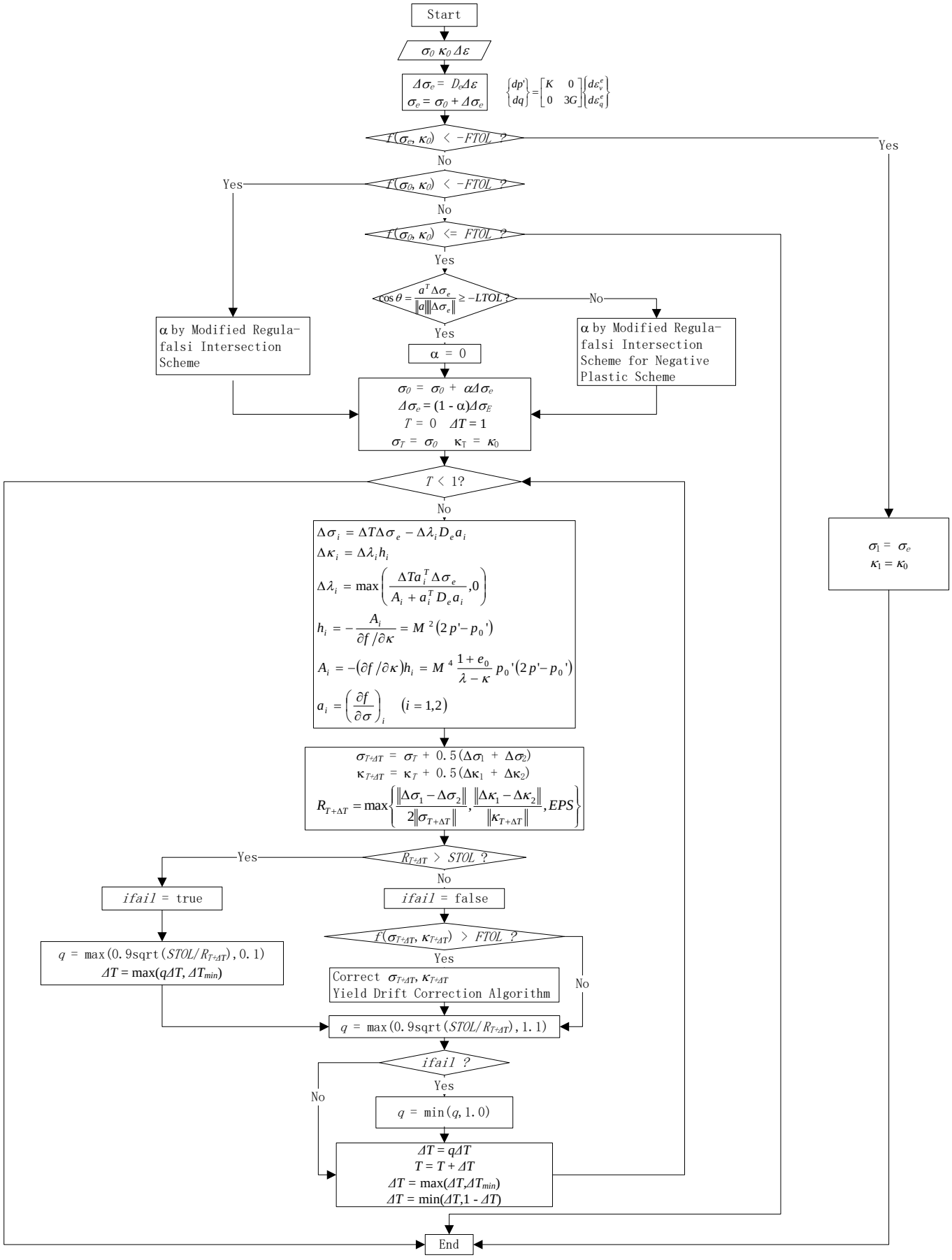

Fig. 5 Flow chart of the explicit method

4. Description of Experiment Data

The input parameters for the MCC model can be calibrated based on the results of hydrostatic compression tests and triaxial tests. According to the results of isotropic compression tests, the isotropic normal consolidation line (NCL) and the unloading reloading line (URL) can be plotted on the *e–lnp′* plane, as shown in Fig. 6.

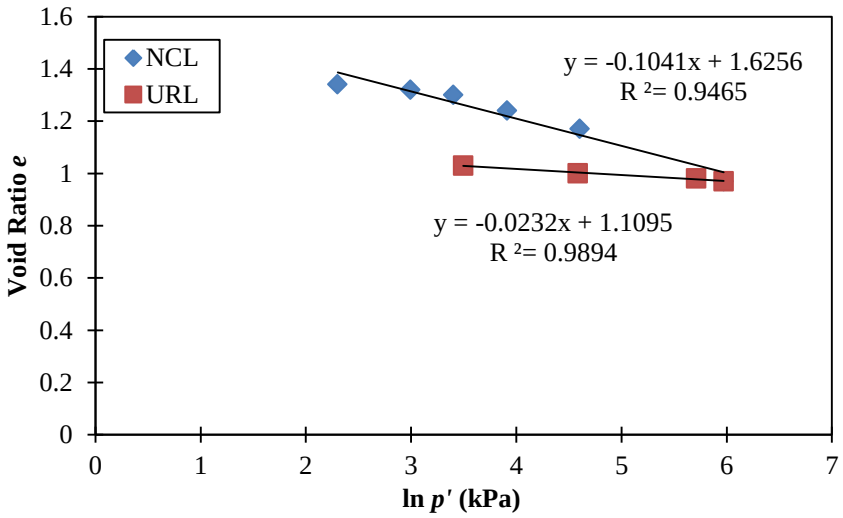

Fig. 6 NCL and URL in the *e–lnp′* plane

Using the linear regression technique, the equations describing the NCL and URL on the *e-lnp′* space can be evaluated as the followings:

NCL: $e = -0.1041 \ln p' + 1.625$ (4.1)

URL: $e = -0.0232 \ln p' + 1.109$ (4.2)

Therefore, the elastic logarithmic bulk modulus $\kappa = 0.0232$; and the plastic logarithmic bulk modulus $\lambda = 0.1041$.

If we assume all the soil samples in the three undrained triaxial tests have reached the critical state, the critical sate line (CSL) on the *p'*-*q* plane can be plotted, as shown in Fig. 7.

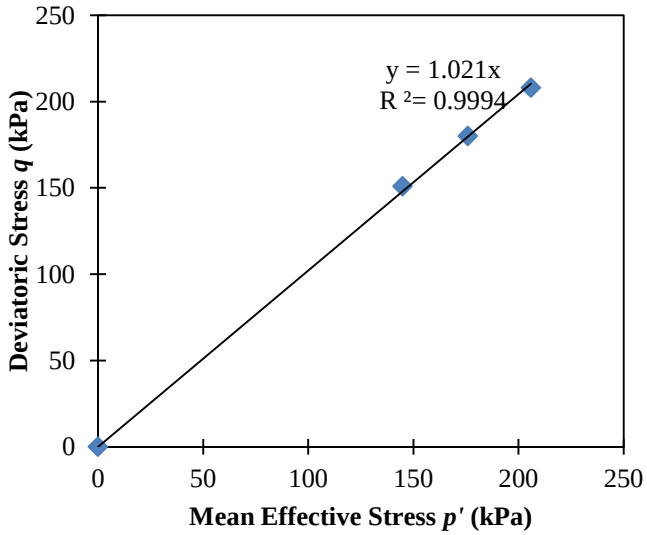

Fig.7 Critical sate line (CSL) on the p'-q space

Using the linear regression technique, the stress ratio *q/p'* at the critical state line $M = 1.021$.

5. Comparison between Experiment and Simulation

5.1 Three undrained triaxial tests

According to the undrained triaxial experiment data, the *p'*-*q*, *q*-ε_a and *u*- ε_a relations can be drawn in Fig. 8 to Fig 10. As shown in Fig.8, the deviatoric stress *q* increases with the deviatoric strain and finally reaches the critical state where *q* no longer increases. As predicted by the MCC model, in the drained condition, the lightly over-consolidated sample tends to contract and the heavily over-consolidated sample experiences contraction first, following by the dilation. Therefore, in Fig.9, because these are the undrained tests, the excessive pore water pressure prevents the contraction and dilation and that is why we can see the change of pore water

pressure. Fig. 10 draws the stress-path of the three samples. Before touching the yielding surface, the deviatoric stress q increases while the mean effective stress p' keeps constant. Afterwards, the stress path bends and touches the critical state line.

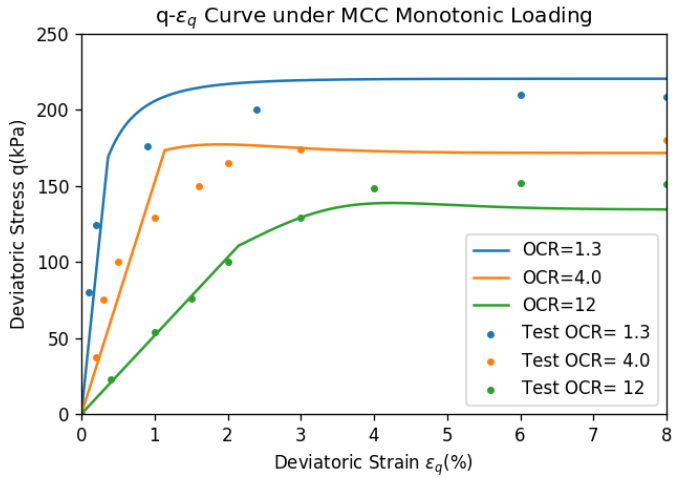

Fig.8 Deviatoric stress vs. deviatoric strain for three samples with different OCR

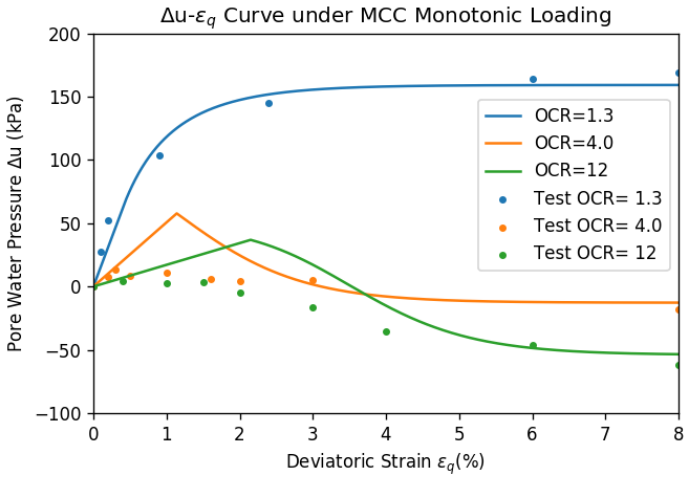

Fig.9 Excessive pore water stress vs. deviatoric strain for three samples with different OCR

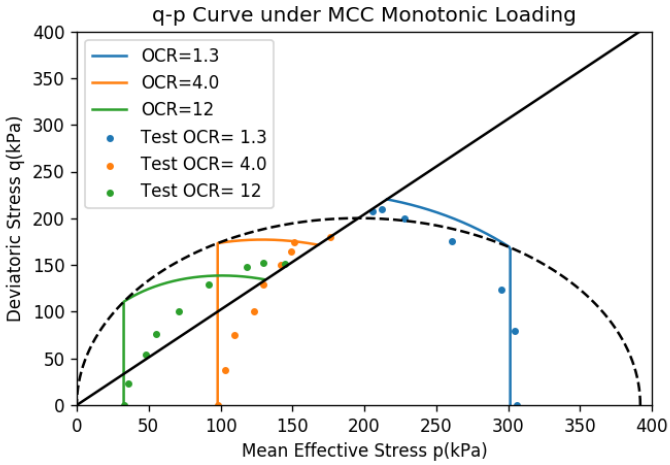

Fig.10 Deviatoric stress vs. mean effective stress for three samples with different OCR

5.2 Cyclic loading

Also, the prediction of cyclic loading are plotted as below. Fig. 11 illustrates the change of deviatoric stress *q* during the 5 cycles of peak-to-peak loading. It can be seen that during the first half-cyclic loading, the yielding surface expand. The coming consequence is that the soil keeps staying in the elastic scope. That is why we can only see a straight line afterwards. Similar result can be seen in the Fig. 12 which describes the pore water pressure during loading and Fig. 13 which plots the stress path during the process.

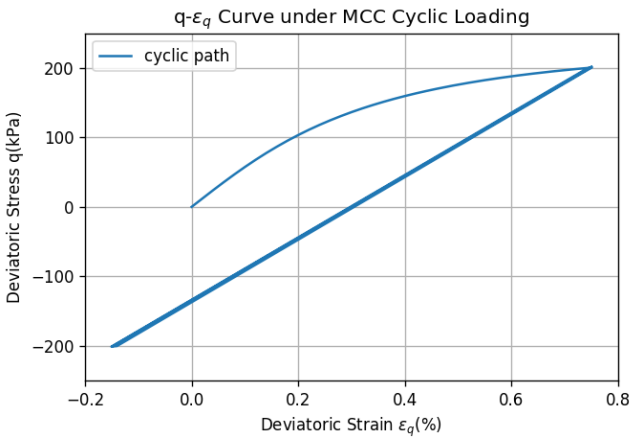

Fig.11 Deviatoric stress vs. deviatoric strain in cyclic loading

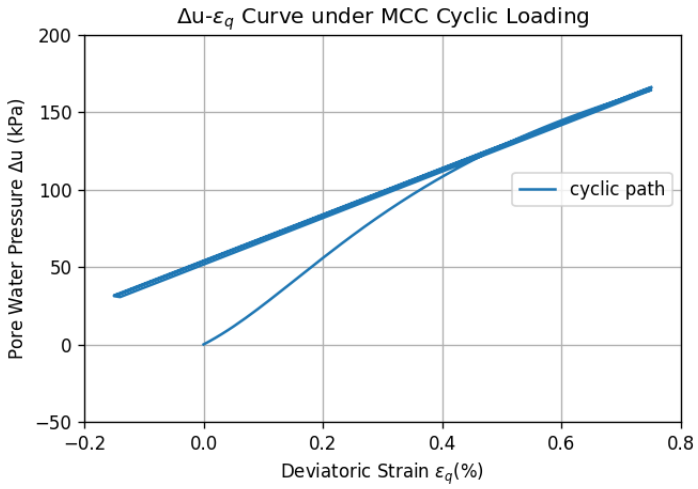

Fig.12 Excessive pore water stress vs. deviatoric strain in cyclic loading

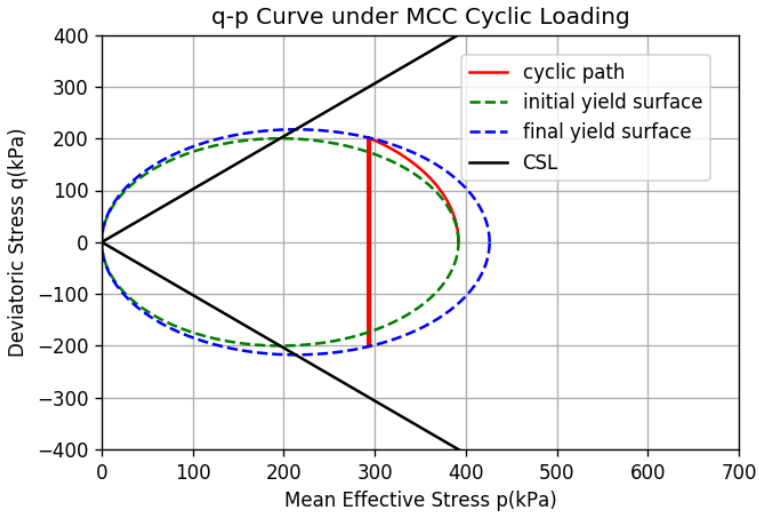

Fig.13 Deviatoric stress vs. mean effective stress for three samples in cyclic loading

6. Discussion

6.1. Comments on the model predictions

The MCC model can predict well the development of deviatoric stress *q* with the deviatoric strain. Fig. 8 shows the stress paths obtained from experiment results and model prediction in

monotonic loading. For different samples with different OCR, they have quite similar performance for deviatoric stress q and finally come to the critical state at similar values.

The MCC model is also able to reproduce the different behaviors of soil samples of different OCRs. In the drained test, the slightly over-consolidated soil (OCR =1.3) would like to contract while the heavily over-consolidated soils (OCR = 4.0 and 12.0) would first experience contraction tendency and then dilation tendency. As shown in Fig, 9, since the undrained condition prevents volumetric change, the slightly over-consolidated soil will generate positive pore water pressure, while the other two will first generate positive pore water pressure, following by the negative one. The tendency of lab tests and simulations are also similar.

However, it should be noted that there are still some discrepancies between the simulation and experiment results quantitatively speaking. First, smaller positive pore water pressure is measured at the very beginning of the shearing process for heavily over-consolidated in the experiments. Second, as shown in Fig. 10, the experimental stress paths are also deviating from the predicted ones. The experimental stress paths would bend at the beginning of the shearing process and the elastic and plastic parts cannot be distinguished.

There are some explanations for the discrepancies between the experiment and predicted results.

(1) It was assumed that there was no plastic deformation before soil reached the yield surface. However, the experimental data showed that plasticity is everywhere.

(2) It was assumed that the Poisson ration remained constant in the MCC model. Actually soil's shear modulus is not proportional to p'.

(3) The plastic work is assumed fully dissipated in the MCC model. However, part of plastic work may be actually stored as “frozen elastic energy” or “stored plastic work”.

(4) Associated flow rule is adopted in the MCC model, which may be unreal.

(5) Soil anisotropy will influence the experimental result.

6.2. Comments on the cyclic loading test

For the normally consolidated soil under cyclic loading, theoretically speaking, the soil will first undergo a plastic deformation process during the first half-cycle from q = 0 to 200 kPa. The yielding surface would expand during the first loading process and consequently the sample stays in the elastic scope during the coming cycles. That is why we can see the curves in Fig. 12 to 15 would remain its state in the straight line.

However, the soil behavior under cyclic loading in fact is more complex. Hysteretic loops in p'-q space and stress-strain relation would be measured due to soil liquefaction. It means that during the cyclic loading, the soil will lose strength and come to liquefaction. Much work has been done by Seed and his coworkers (Seed et al., 1976 and Seed, 1979). However, the MCC model seems not suitable in the modeling for soil behavior under cyclic loading. Soil will never fail after cyclic loading and it is because that the anisotropy is not taken into account (Borja, 2001).

7. Conclusions

In this report, the simulation results of soil behaviors under triaxial compression and cyclic loading conditions were presented. The main findings are as followings.

(1) The MCC model is suitable to simulate the soil behavior under the triaxial conditions. The predicted stress path, stress-strain relation and pore water pressure show pretty good agreement with those measured in experiments. The difference between the behaviors of soil samples with different OCRs are also reflected in the simulation results.

(2) Some discrepancies exist between the predicted and experiment results of soil behavior under triaxial compression conditions. This may be related to the unrealistic assumptions and simplifications of the MCC model.

(3) The MCC mdeol does not consider the effect of soil liquefaction. Therefore under cyclic loading, the soil still keeps in the elastic scope and cannot reach the liquefaction state. Hence, it is not so suitable for the MCC model to predict the soil behavior under cyclic loading or dynamic condition.

References

J.D. Zhao. (2018). Lecture notes of CIVL 5730: Theoretical and computational soil mechanics. HKUST

Sloan SW. Substepping schemes for the numerical integration of elastoplastic stress–strain relations. Int J Numer Methods Eng. 1987;24(5):893-911.